Effect of water radiolysis and complexing species on the leaching of zirconolite

M. Tribet[1,2], N. Toulhoat[1*], N. Moncoffre[1], C. Jégou[2], G. Leturcq[2], C. Corbel[3], P. Toulhoat[4**]

[1] *Institut de Physique Nucléaire de Lyon (IPNL), Université de Lyon, Université Lyon1, CNRS/IN2P3, 4 Rue E. Fermi, 69622 Villeurbanne cedex, France*
[2] *CEA/DEN/DTCD.SECM/LMPA, Marcoule, BP 17171, 30207 Bagnols sur Cèze cedex, France,* magaly.tribet@cea.fr
[3] *CEA/DSM/DRECAM/LSI, École Polytechnique, 91 128 Palaiseau, France*
[4] *Université de Lyon, Université Lyon1, CNRS/ISA, UFR de Chimie Biochimie, 69622 Villeurbanne cedex, France*
** CEA/DEN/Saclay, 91191 Gif sur Yvette cedex, France*
*** INERIS, Parc Technologique Alata, BP2 F-60550 Verneuil en Halatte, France*

Abstract *– Zirconolite is one of the matrices considered for the confinement of minor actinides in case of deep geological disposal. Its chemical durability has been studied during dissolution under charged particle-induced water radiolysis (He^{2+} and proton external beams) to identify possible effects on dissolution rates and mechanisms. Two experimental geometries have been used to assess the influence of the solid irradiation on one hand and the total deposited energy into water on the other hand. These irradiations have been performed on polycrystalline zirconolites ($Ca_{0.8}Nd_{0.2}ZrTi_{1.8}Al_{0.2}O_7$) in pure water or in presence of complexing ions such as F^-. The sample dissolution has been monitored through the release of cations. Under radiolysis, an increase in the Zr, Ti and Nd releases of one order of magnitude has been observed compared to results obtained without radiolysis. The presence of complexing species has induced an additional increase of two orders of magnitude in the Ti and Zr releases.*

INTRODUCTION

In the hypothesis of a geological disposal of nuclear wastes, natural groundwater would be the principal vector of dissemination of the radioactive elements. Minor actinides resulting from enhanced reprocessing of spent fuel could be contained in a specific matrix, able to incorporate them in its structure and having a good stability over geologic periods of time. The favoured incorporation of tri- and tetra-valent actinides in the zirconolite structure by substitution at calcium and zirconium sites, combined with a very high chemical durability of this material, makes it a good candidate for the containment of minor actinides [1-4].
The dissolution of both natural and synthetic zirconolites has been studied by several authors over the last fifteen years [5-9]. The aqueous alteration kinetic of zirconolite is very slow over a wide pH (2-13) and temperature (25-200 °C) range. The initial dissolution rate R_o has been evaluated in dynamic conditions (100 °C, distilled water) to about 10^{-2} g.m^{-2}.day^{-1} using calcium as a dissolution marker and 10^{-6} g.m^{-2}.day^{-1} using neodynium (the actinide simulant) [8]. The alteration is rapidly stopped by the formation of a very thin, insoluble, decalcified film at the mineral/water interface. This passivation layer protects the surface from further alteration [7]. Concerning irradiation effects, leaching experiments performed on fully metamict natural Th-enriched zirconolite as well as leaching experiments performed on synthetic ceramics irradiated by external heavy-ion beams show that the chemical durability is not fundamentally modified [6, 8].
However, concerning chemical species present in groundwater, organic complexing species can modify the dissolution mechanisms of zirconolite. The effects of citric acid on zirconolite dissolution have been studied, citrate ions being well known to form very stable complexes with Zr^{4+}, Ti^{4+} and Nd^{3+} [9]. It has been shown that the presence of such a complexing species induces an increase in the Ti and Zr release rates of one and three orders of magnitude respectively, and thus, in this case, dissolution becomes congruent.

However, in case of long term disposal, another parameter, which could have an influence on the dissolution mechanisms, is the water radiolysis induced by He^{2+} irradiation at the zirconolite/water interface. Water radiolysis induces the formation of short-lived radicals such as $HO^\bullet$, $H^\bullet$, $HO_2^\bullet$ that recombine after 10^{-6} s to form stable molecular species (mostly gaseous H_2 and soluble H_2O_2) [10].

We have investigated the effects of external irradiation induced water radiolysis on the leaching of a synthetic zirconolite, using accelerated He^{2+} and proton beams. We assume here that He^{2+} and protons with comparable energies provide qualitatively similar effects in water with respect to the quantity and the nature of the formed radicals. Two different irradiation geometries have been studied: in the first one, sample irradiation and water radiolysis are coupled whereas, in the second one, the solid is not irradiated and there is only water radiolysis. Previous papers have shown that the dissolution of the zirconolite surface is enhanced during radiolytic dissolution induced by charged particle irradiation [11, 12]. In this paper, we focus on the effects of complexing species such as fluorine on the zirconolite dissolution under radiolysis conditions.

EXPERIMENTAL

Samples

The studied material is a nearly pure Nd-doped sintered zirconolite [7]. Its formula is (99.5 vol % $Ca_{0.8}Nd_{0.2}ZrTi_{1.8}Al_{0.2}O_7$), with a minor $ZrTiO_4$ phase (0.5 vol %), Nd being used to simulate actinide doping [3]. A density of (4.63±0.05) $g.cm^{-3}$ has been measured. The zirconolite surface has been polished to a 1 µm finish.

Irradiation Geometries and Conditions

Two different geometries have been studied. In the first one, called the CERI geometry, implemented at the CERI (Centre d'Etudes et de Recherches par Irradiation, Orléans, France) cyclotron, we have used a charged particle beam passing through the sample and inducing radiolysis of the solution at the opposite sample surface. In this geometry, there is no water circulation: the leaching takes place in static conditions. The experimental device has been extensively described in a previous article [13]. In this kind of experiment, ionization and electronic excitation occur in the sample as well as in the water at the very near sample/water interface.

In the second geometry, called the IPNL geometry, implemented at the 4 MV Van de Graaff accelerator facility of the IPNL (Institut de Physique Nucléaire de Lyon, France), the charged particle beam enters directly the water through a Havar® window and stops before reaching the sample. In this last configuration, the solid is not irradiated. A closed water circulation allows the evacuation of the bubbles (H_2) formed during the irradiation in the narrow water film located between the Havar® window and the zirconolite sample ((175±5) µm thick). This experimental device has also been extensively described in a previous article [13]. In the present study, a heating device has been added in order to heat the water up to 50 °C. The temperature in the very thin irradiated water film is controlled by a thin thermocouple (diameter of 0.64 mm).

Several kinds of experiments have been performed:

- in each geometry using pure water;
- in the CERI geometry, where the solid is also irradiated, Teflon pieces from the cell have in some cases been irradiated, inducing the release of fluoride species into water. These species are known to form very stable complexes with Zr^{4+}, Ti^{4+} and Al^{3+} [14, 15, 16]: thus, these experiments have allowed us to study the effects of the presence of complexing species on the zirconolite dissolution.

For each experiment, the energy deposited into water, $E_{deposited}$, (in J), has been calculated using equations (1) and (2):

$$E_{deposited} = number\ of\ particles \times T \times E_{water} \times (1.6\times10^{-19}) \quad (1)$$

$$number\ of\ particles = \frac{I \times \Delta t}{1.6\times10^{-19}} \quad (2)$$

Where:
- I is the beam intensity (30 nA);
- Δt (in s) is the irradiation duration;
- E_{water} (in eV) is the beam energy when it emerges into water;
- T is the Si grid transparency [13] ((30±4) %). This grid is used only for experiments performed in the IPNL geometry;
- (1.6×10^{-19} C) is the electron charge.

Solving equations (1) and (2) for both geometries leads to the following simplified relations:

- For experiments performed in the IPNL geometry, the deposited energy, expressed in J, only depends on the irradiation duration, Δt, expressed in hours:

$E_{deposited}$ = (114±8) × Δt

For experiments performed in the CERI geometry, as the ion beam passes through the sample before stopping into water, the deposited energy depends both on the irradiation duration, Δt (in hours) and on the sample thickness:

$E_{deposited} = (52.2 \pm 2.7) \times \Delta t \times E_{water}$

where here, E_{water} is expressed in MeV.

Table I summarizes, for the different experiments and in presence of complexing species, the sample thickness range, the temperature, the irradiation duration range and fluence range, the beam energy range, the particle ranges (Rp) and the range of the energy deposited into water. Concerning experiments performed into pure water, a similar table has been presented in a previous article [12].

TABLE I. Irradiation conditions of the zirconolite samples at the CERI facility under complexing conditions.

Experimental geometry	CERI
Number of irradiated samples	6
Temperature (°C)	20
Sample thickness (μm)	408 - 417
Beam energy entering water (keV)	6200 - 7850
Rp (μm)	58 - 82
Irradiation duration (hours)	1.5 to 7
Fluence ($at.cm^{-2}$)	$1.8.10^{15}$ to $8.3.10^{15}$
Deposited energy into water (J)	625 - 2888

Cation analysis

The cation concentrations (Al, Ca, Nd, Ti and Zr) released during the leaching of the zirconolite surface have been analyzed in the irradiated solutions as well as in solutions having being in contact with zirconolite surfaces for duration identical to the irradiation time (which are "blank" experiments). After each experiment, the leachate has been separated into two fractions: soluble cations and/or cations retained on a colloidal fraction have been measured on a fraction filtered at 0.45 μm (first fraction) and soluble cations have been measured on a fraction ultrafiltered at 0.020 μm (second fraction). Both fractions have been acidified with nitric acid 2 $mol.L^{-1}$.

After each experiment, the device has been rinsed with nitric acid 0.5 $mol.L^{-1}$. This last solution is identified as the rinse solution. The total cation concentration corresponds to the sum of the quantities measured in the filtered solution and in the corresponding rinse solution.

The analyses have been performed:

- for pure water experiments, with a ICP-MS Agilent 7500 CE system at the Ecole Normale Supérieure of Lyon (France). The limits of detection (LOD) are of 0.01 $\mu g.L^{-1}$ for Nd, Ti and Zr, which corresponds to a LOD of 2×10^{-10} $mol.L^{-1}$ for Ti, and 10^{-10} $mol.L^{-1}$ for Nd and Zr. Uncertainties are about ± 25 %;
- for experiments where fluoride species have been released into water, with a ICP-MS "Element 1" (Thermo) at the Service Central d'Analyses (Vernaison, France). For the less soluble cations, the detection limits (LOD) are of 0.2 $\mu g.L^{-1}$ for Nd and Zr and of 0.5 $\mu g.L^{-1}$ for Ti, which correspond to a LOD of 2×10^{-9} $mol.L^{-1}$ for Nd and Zr, and 10^{-8} $mol.L^{-1}$ for Ti. Uncertainties are about ± 10 %.

The calcium and aluminum releases have to be considered as order of magnitudes only in the following discussion: indeed, aluminum and mainly calcium concentrations have been affected by an external contamination, arising from powdered gloves and ambient atmosphere. Concerning aluminum, the contamination is more important for the CERI than for the IPNL experiments.

Anion analysis

The amount of fluoride species in the solutions has been measured in the filtered fraction. The analyses have been performed with an ionic chromatography Dionex DX.500 system at the Service Central d'Analyses. The LOD is of 10 $\mu g.L^{-1}$. Uncertainties are about ± 10 %.

The nature of fluoride species and their corresponding concentration in the irradiated solution are given in Table II. This table shows that the fluoride ion concentration is about two orders of magnitude higher than the other ion concentrations.

TABLE II. Nature and corresponding concentration of the mean ions measured in the irradiated solutions after a 6/7 hours irradiation duration. These values vary as function of the irradiation duration: for a 2 hours irradiation duration, concentrations are one order of magnitude below those given in this table.

Ions measured	Mean concentration ($mg.L^{-1}$)	Mean concentration ($mol.L^{-1}$)
F^-	22.80	1.2×10^{-3}
trifluoroacetate	2.26	2×10^{-5}
acetate	1.77	3×10^{-5}
formiate	0.45	10^{-5}

Environmental Secondary Electron Microscopy (ESEM)

Environmental mode has been used for the zirconolite sample surface analysis in order to avoid any modification of the sample surface due to metallization.

ESEM analysis have been performed with a Philips XL30 microscope at the Consortium Lyonnais de Microscopie Electronique (Lyon, France) or at the Centre de Recherche sur les Matériaux à Haute Température (Orléans, France), using a 15 kV accelerating voltage and with a 2 Torr water pressure.

RESULTS

Experiments Performed in Pure Water

These experiments have been performed in both geometries and allowed to monitor zirconolite surface dissolution with respect to:

- water radiolysis solely (IPNL geometry),
- coupled water radiolysis and solid irradiation (CERI geometry).

The results have been presented in previous articles [11, 12] and are summarized in Figure 1 and Figure 2.

Firstly, we have shown that under radiolysis, an increase of one order of magnitude is observed for the Ti, Nd and Zr releases [11].

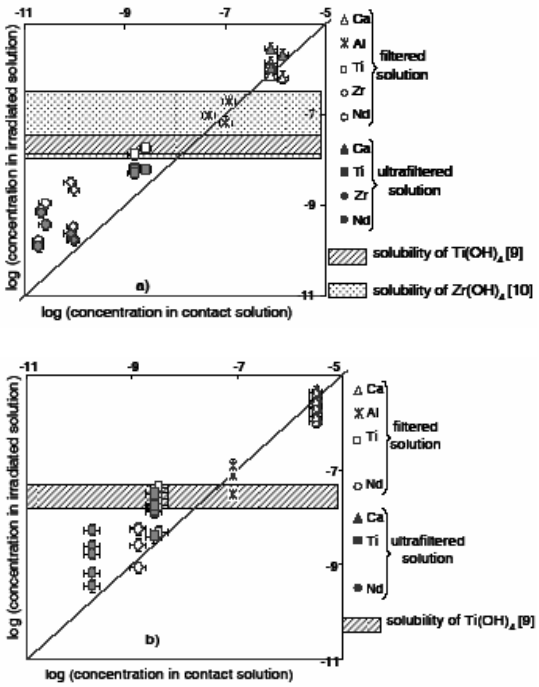

Figure 1. Cation concentrations (Ca, Al, Nd, Ti and Zr) measured in $mol.L^{-1}$ in the irradiated solutions versus their concentrations measured in the contact solutions for filtered (open symbols) and ultrafiltered solutions (closed symbols) [11]. Each plot corresponds to an irradiated sample. The solid line represents the graph bisector. a) Results obtained for the CERI experiments, when the beam passes through the sample; b) results obtained for the IPNL experiments. In this case, the values for the contact solution are the average concentrations obtained from several experiments and the error bar corresponds to the standard deviation. The solubility domains for $Ti(OH)_4$ and $Zr(OH)_4$ are represented by the dashed areas and the dotted area respectively.

Secondly, focusing on the evolution of the elemental releases versus deposited energy (figure 2), the main conclusions are the following [12]:

- Without any solid irradiation (IPNL geometry), the evolution of the elemental releases versus deposited energy shows that dissolution is first kinetically and then thermodynamically controlled. Dissolution effects are accelerated under radiolysis during the kinetic period: comparing to observation made in the literature without radiolysis, rates are higher under radiolysis and the kinetic period is lower [7, 8, 12]. This observation may correspond to an active attack by the radiolytic species (H_2O_2 and radicals) on the cations [17,

18]. We have also pointed out that the solubilities of Ti and Zr hydroxides control the elemental concentrations in the leachate. The Nd releases are controlled by the $Ti(OH)_4$ solubility. However, the alteration layer could not be observed by solid analysis because of its too thin thickness (about 2 nm at maximum [11]).

- For the experiments coupling solid irradiation and water radiolysis (CERI geometry), no thermodynamic equilibrium has been observed (figure 2 c)). Two hypotheses could explain such a behaviour: first, the fact that the Ti and Zr releases begin to reach the hydroxide solubilities limit values only for the highest deposited energies ($E_{deposited} \approx 900$ J) could mean that higher deposited energies would be necessary to reach the thermodynamic stage. Second, as the solid irradiation leads to ionizations in the solid, particularly near the sample/water interface, these ionizations could induce a modification in the chemical equilibria.

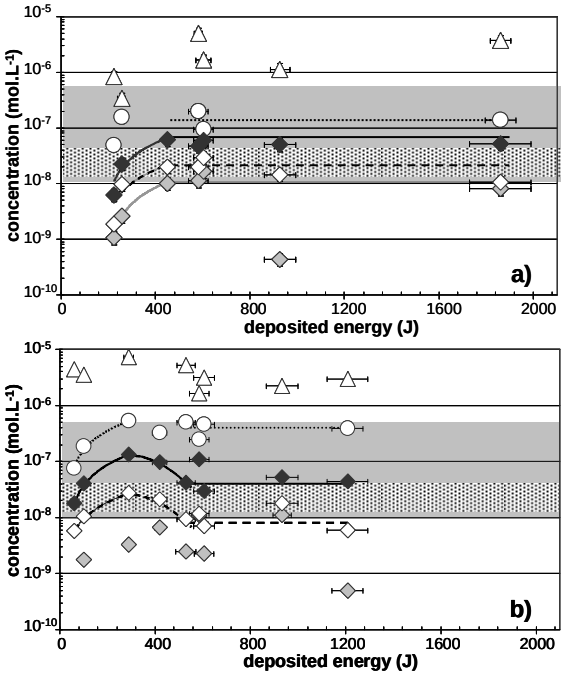

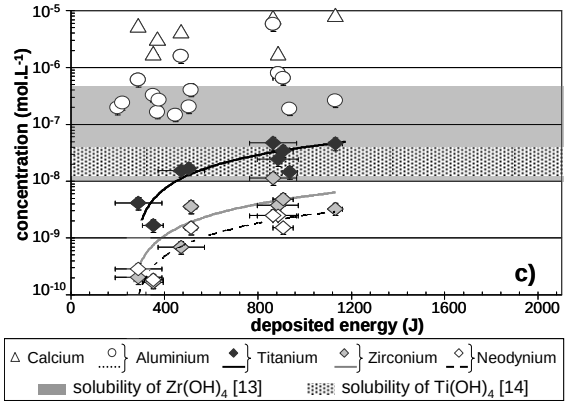

Figure 2. Total elemental concentrations released under radiolysis (in log scale) versus the deposited energy for experiments realized at 20 °C (a), at 50 °C (b) and for experiments coupling water radiolysis and solid irradiation (c). The solubility domains for $Zr(OH)_4$ and $Ti(OH)_4$ are represented by the grey area and the dotted area. Solid, dotted and dashed lines represent the least square linear regressions of the experimental data. Horizontal lines are put by way of guideline [12].

Experiments Performed in Water Containing Fluoride Species

Figure 3 presents the detailed results obtained for irradiated solutions containing the fluoride species described in Table II. It represents the cation concentrations measured in the irradiated filtered solutions versus the cation concentrations measured in the contact solutions ("blank" experiments, into pure water). In this figure, the solid line represents the graph bisector. These experiments have been performed in the CERI geometry (coupled water radiolysis and solid irradiation).

Comparing Figure 3 and Figure 1 b., we can notice that the presence of fluoride species induces an increase of two orders of magnitude of the Ti and Zr releases as well as an increase of one order of magnitude of the Al releases.

As for Nd, the amounts released are of the same order of magnitude in presence of fluoride species compared to pure water (about 10^{-8} $mol.L^{-1}$). Therefore, Nd releases are not affected by the presence of the fluoride species.

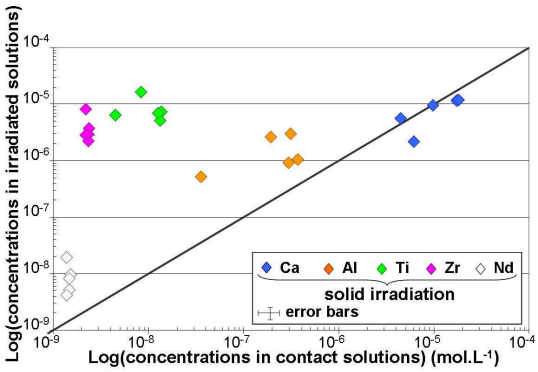

Figure 3. Cation concentrations (Ca, Al, Nd, Ti and Zr) measured in mol.L^{-1} in the irradiated solutions versus their concentrations measured in the contact solutions for solutions containing fluoride species. Each plot corresponds to an irradiation experiment. The solid line represents the graph bisector.

Moreover, comparing these cation concentrations to fluoride species concentrations given in Table II lead to the following comments:

- Al, Ti and Zr concentrations are of the same order of magnitude than trifluoroacetate and acetate ion concentrations (about 10^{-5} mol.L^{-1});
- Al, Ti and Zr concentrations are two orders of magnitude lower than fluoride ion concentrations: fluoride ions are then in large excess.

Thus, the formation of Al, Ti and Zr trifluoroacetate, acetate and fluoride complexing species can explain this large increase in the cation releases.

Figure 4 presents the cation concentrations released in the irradiated filtered and ultrafiltered solutions containing fluoride species versus the energy deposited in the solution by the He^{2+} ion beam. An analysis of the surface topography by ESEM is presented in figure 5, in order to complete the observations deduced from figure 4.

Figure 4 shows that the evolution of the releases in the filtered solutions versus the deposited energy is the same for all the species, including fluoride ions: this increase versus deposited energy, observed for all experimental data, can be fitted by a least square exponential regression. This indicates that, for each ion, the releases can be described by a first-order kinetic law. As all the exponential regressions are parallel, the rate constant is the same for all the species which indicates that the elemental releases are linked to the presence of fluoride ions.

Figure 4 also shows that:

1) concerning the filtered solution, the releases are similar and congruent for all elements except Nd. Moreover, the grain boundaries are revealed during dissolution (Figure 5b). All these data are in agreement with the work done by P. McGlinn for the zirconolite in presence of an organic complexing species [9].

2) concerning the ultrafiltered solutions, the releases of Zr and Nd are different from those in the filtered solutions. This difference indicates the presence of a colloidal fraction retaining Nd and Zr. These colloids have been observed by ESEM (figure 5c and d). As for the Ti, the releases do not differ from the filtered ones. Ti does not enter the colloidal fraction anymore, compared to the results obtained in pure water [11, 12]. In presence of these complexing species, Ti remains in the solution as a soluble complex.

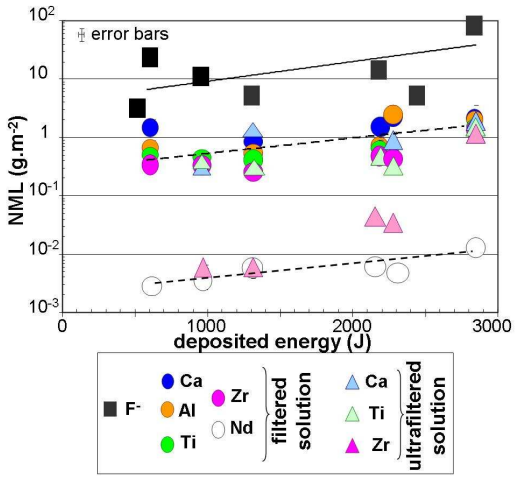

Figure 4. Elemental concentrations of Ca (blue), Al (orange), Ti (green), Zr (pink) and Nd (white), and F- concentration (black), in the filtered solutions (round shaped) and the ultrafiltered solutions (triangles), versus the deposited energy, for experiments performed in the CERI geometry (coupled water radiolysis and solid irradiation). The concentrations are expressed in normalized mass losses (NML) unit (g.m^{-2}) and represented in log scale. For the

fluoride ions, the conversion to NML unit takes into account the Teflon irradiated surface (0.0157 cm^{-2}). Nd values in ultrafiltered solutions are not given because they are situated below the LOD. Solid, dotted and dashed lines represent the least square exponential regressions of the experimental data (respectively fluoride, then Ca, Ti, Zr, Al and finally, Nd).

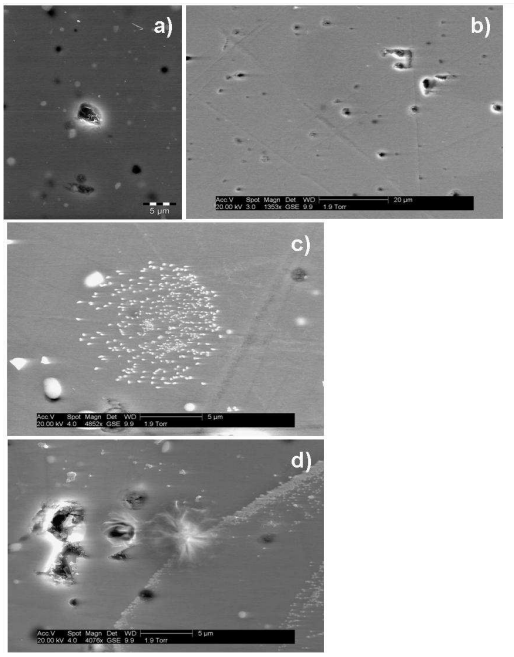

Figure 5. ESEM analyses of a virgin zirconolite sample (image a) and of an irradiated and leached sample (images b to d) in presence of fluoride species (fluence of 7.8×10^{15} at.cm^{-2}, 7 hours, 2290 J of deposited energy). Image b. represents the general aspect of the sample surface. Images c. and d. show deposits punctually observed on the irradiated surface.

CONCLUSIONS

Zirconolite is one of the matrices foreseen for the containment of minor actinides in the hypothesis of a geological disposal of nuclear wastes. We have performed experiments in order to study the dissolution of zirconolite surface with respect to the effects of water radiolysis solely on one hand, and, the effects of coupled water radiolysis and solid irradiation on the other hand. The experiments have been first performed in pure water and then in solutions containing complexing agents.

For the experiments performed in pure water [11,12] in the IPNL geometry (water radiolysis solely), we have shown that the zirconolite dissolution is rapidly stopped and that the leaching process is thermodynamically controlled after few hours by the $Ti(OH)_4$ and the $Zr(OH)_4$ solubilities [12]. On the contrary, in the CERI geometry (coupled water radiolysis and solid irradiation), the dissolution mechanisms seem to be different: no thermodynamic control has been observed [12] and a colloidal fraction containing $Zr(OH)_4$ and $Ti(OH)_4$ has been evidenced [11]. Two hypotheses could explain this behaviour: first, higher deposited energies would be necessary to reach the thermodynamic stage. Therefore, complementary experiments performed at higher deposited energy would be necessary to eventually observe a thermodynamic step in this geometry. Second, the solid irradiation leads to ionizations in the solid, particularly near the sample/water interface. These ionizations could induce a modification in the chemical equilibria, and could also explain the presence of colloids. However, a main conclusion can be drawn: in pure water, even under radiolytic conditions, the zirconolite remains a good candidate for the containment of minor actinides. The equivalent thickness of alteration calculated from Nd releases is less than 2 nm, corresponding to about 5 atomic layers [11]!

The experiments performed in solutions containing fluoride complexing species (F-, acetate, trifluoroacetate, formiate) have been performed in the CERI geometry (coupled water radiolysis and solid irradiation). The influence of such species has to be kept in mind in case of presence of granitic waters or of fluorinated wastes (Teflon tubes and joints). We have shown that these complexing species enhance the elemental releases by a factor of 100 for Ti and Zr, and by a factor of 10 for Al, compared to results obtained in pure water. In this case, the zirconolite dissolution becomes congruent for all elements except Nd, which does not seem to be affected by the presence of these species. Moreover, only the kinetic step has been observed, whereas the thermodynamic stage has not been evidenced. The elemental releases and the fluoride concentration follow a first-order kinetic law with a constant rate. The zirconolite dissolution can thus be linked to the presence of these fluoride species and can be explained by the formation of complexes with Ti, Zr and Al.

Further experiments at higher deposited energy would be necessary to complete the kinetic study and observe a change in the kinetic law.

ACKNOWLEDGMENT

The authors would like to thank all the persons who have helped during experiments: the "Accelerator Team": C. Peaucelle, A. Gardon, R. Fillol, Y. Champelovier, A. Perrat-Mabilon for their help at the IPNL facility; M. Guiset, S. Ancelin, T. Mennecart and E. Mendes for their help at the CERI facility; P. Telouk and C. Douchet for the ICP MS analysis performed at the ENS of Lyon, and J.L. Imbert and L. Dutruch for the ICP MS analysis performed at CNRS/SCA and E. Veron (CRMHT) and A. Perrat (CLYME) for the ESEM analysis.

REFERENCES

1. C. FILLET, J. MARILLET, J. L. DUSSOSSOY, F. PACAUD, N. JACQUET FRANCILLON, J. PHALIPPOU, *Ceramic Trans.*, **87**, 531 (1998).

2. T. ADVOCAT, C. FILLET, J. MARILLET, G. LETURCQ, J. M. BOUBALS, *Mat. Res. Soc. Symp. Proc.*, **506**, 55 (1998).

3. G. LETURCQ, *Alteration et comportement à long terme de différentes classes de matériaux innovants pour le confinement des radionucléides à vie longue,* PhD thesis, University Toulouse III, France, (1998).

4. G. LETURCQ, T. ADVOCAT, K. HART, G. BERGER, J. LACOMBE, A. BONNETIER, *Am. Mineral.,* **86**, 871 (2001).

5. C. GUY, F. AUDUBERT, J. E. LARTIGUE, C. LATRILLE, T. ADVOCAT, C. FILLET, J. MARILLET, G. LETURCQ, J. M. BOUBALS, *C. R. Physique*, **3**, 827 (2002).

6. A. E. RINGWOOD, V. M. OVERSBY, S. E. KESSON, W. SINCLAIR, N. WARE, W. HIBBERSON, A. MAJOR, *Nucl. Chem. Waste Management*, **2 issue 4**, 287 (1981).

7. G. LETURCQ, P. J. MCGLINN, C. BARBE, M. G. BLACKFORD, K. S. FINNIE, *Applied Geochem.,* **20**, 899 (2005).

8. C. FILLET, T. ADVOCAT, F. BART, G. LETURCQ, H. RABILLER, *C. R. Chimie*, **7**, 1165 (2004).

9. P. J. McGLINN, T. McLEOD, G. LETURCQ, Z. ALY, M. G. BLACKFORD, Z. ZHANG, H. LI, G. R. LUMPKIN, *Mat. Res. Soc. Symp. Proc.*, **807**, 219 (2004)

10. V. TRUPIN-WASSELIN, *Processus primaires en chimie sous rayonnement. Influence du TEL sur la radiolyse de l'eau,* PhD thesis, University Paris-Sud, France, (2000).

11. M. TRIBET, N. TOULHOAT, N. MONCOFFRE, C. JEGOU, G. LETURCQ, C. CORBEL, P. TOULHOAT, *Mat. Res. Soc. Symp. Proc.*, **985**, (2007).

12. M. TRIBET, N. TOULHOAT, N. MONCOFFRE, C. JEGOU, G. LETURCQ, C. CORBEL, P. TOULHOAT, *Radiochimica Acta*, to be published (2008).

13. M. TRIBET, S. GAVARINI, N. TOULHOAT, N. MONCOFFRE, A. CHEVARIER, C. JEGOU, G. LETURCQ, C. CORBEL, P. TOULHOAT, *Radiochimica Acta,* **94**, 585 (2006)

14. P. L. BROWN, L. CURTI, B. GRAMBOW, *Chemical thermodynamics of zirconium*, Elsevier, Chemical Thermodynamics, **8**, (2005).

15. L. CIAVATTA, A. PIROZZI, *Polyhedron*, **2 n°8**, 769 (1983).

16. G. MICHARD, *Equilibre chimique dans les eaux naturelles*, Publisud, (1989).

17. H. MUNAKATA, Y. OUMI, A. MIYAMOTO, *J. Phys. Chem.*, **B105**, 3493 (2001).

18. E. FOIS, A. GAMBA, E. SPANO, *J. Phys. Chem,*. **B108**, 9558 (2004).